DOE/BC/14899-32
Distribution Category UC-122

Pore Level Visualization of Foam Flow in a Silicon Micromodel

SUPRI TR 100

By
F. Woody
M. Blunt
L. Castanier

January 1996

Work Performed Under Contract No. DE-FG22-93BC14899

Prepared for
U.S. Department of Energy
Assistant Secretary for Fossil Energy

Thomas B. Reid, Project Manager
Bartlesville Project Office
P.O. Box 1398
Bartlesville, OK 74005

Prepared by
Stanford University
088 Green Earth Sciences
Stanford, CA 94305-2220

TABLE OF CONTENTS

Abstract

This paper is concerned with the behavior of foam in porous media at the pore level. Identical, heterogeneous silicon micromodels, two dimensionally etched to replicate flow in Berea Sandstone, were used. The models, already saturated with varying concentrations of surfactant and, at times, oil were invaded with air. Visual observations were made of these air displacement events in an effort to determine foam flow characteristics with varying surfactant concentrations, and differing surfactants in the presence of oil. These displacement events were recorded on video tape. These tapes are available at the Stanford University Petroleum Research Institute, Stanford, California.

The observed air flow characteristics can be broadly classified into two: continuous and discontinuous. Continuous air flow was observed in two phase runs when the micromodel contained no aqueous surfactant solution. Air followed a tortuous path to the outlet, splitting and reconnecting around grains, isolating water located in dead-end or circumvented pores, all without breaking and forming bubbles. No foam was created.

Discontinuous air flow occurred in runs containing surfactant - with smaller bubble sizes appearing with higher surfactant concentrations. Air moved through the medium by way of modified bubble train flow where bubbles travel through pore throats and tend to reside more statically in larger pore bodies until enough force is applied to move them along. The lamellae were stable, and breaking and reforming events by liquid drainage and corner flow were observed in higher surfactant concentrations. However, the classic snap-off process, as described by Roof (1973) was not seen at all.

With oil, we saw coarser bubble texture along with stable water lenses between

gas. Events consistent with the drainage of thin spreading oil layers, as well as the collapse of a water film between oil and gas were observed.

Section 1.
INTRODUCTION

Steam injection is the most widely used enhanced oil recovery technique in the petroleum industry. Some of its applications include carbon dioxide flooding, drilling, and acidizing. One characteristic of steam injection is its suitability for heavy oil reservoirs, where other methods, such as waterflooding, often fail. The injected steam has a much lower density and viscosity than the oil and water it is attempting to displace. This often results in severe gravity over-ride and channeling through high permeability zones, leaving the bottom of the formation and low permeability zones unswept. Foams have been used as a method of mobility control in steam floods, mitigating the problems of channeling and over-ride and resulting in an efficient displacement.

At present, the basic phenomena by which foam flooding works is not known. In particular, it is unclear under what circumstances injected surfactant forms a stable foam and how it reacts with the oil phase. In this study, foam generation occurred through the injection of air into a micromodel saturated with an aqueous solution of surfactant. However, lacking is a quantitative description of foam flooding based on a knowledge of the pore level processes by which the oil is displaced. It is our hope that this understanding can be used to develop a mathematical model of foam flooding that can be used to predict performance at the field scale.

This project has attempted to study the pore level processes in foam flooding in a

silicon micromodel. The micromodel is an exact representation of a slice through a Berea sandstone etched onto a silicon wafer. It honors the microscopic heterogeneity of the rock, but, being two dimensional, loses some of the continuity of a three dimensional sample.

Initial experimentation involved the saturation of this silicon micromodel with an aqueous solution of surfactant and deionized water. This liquid medium is then invaded by air and observed. Varying concentrations of the surfactant, an alpha-olefin sulfonate (AOS 1618) allowed for the viewing of various flow mechanisms and provided valuable insights into the area of foam propagation. The flow mechanisms observed in the two phase runs included bubble train flow and bubble breaking and reforming. These experiments also provided a base case for comparison with three phase work (including oil) also conducted.

Further research incorporated oil (decane) as a residual component in one of the surfactant ladened mediums mentioned above. With a knowledge of the two phase mechanisms already seen in initial experimentation, the objective was simply to determine the effects residual oil saturation might have on foam generation and propagation. In addition, this experiment was repeated at similar active weight concentrations with a more spreading inhibitive surfactant (B1333, a fluoroalkyl sulfobetaine) than the alpha-olefin sulfonate for further insight into foam behavior. It is clear from the runs, that oil has a deleterious affect on foam stability, and consequently, debilitates generation and propagation mechanisms.

As a prelude to these experiments, a literature survey of previous studies on foam flow with and without the presence of oil, as well as the use of micromodels themselves was conducted. This survey is given in the following section.

Section 2.
LITERATURE SURVEY

There has been a great deal of work published concerning foam research. Marsden (1977, 1986) conducted a thorough review of the early work on the selective blockage of fluids in thermal recovery projects. In such projects, foam applications were prominent. As this current research effort is concerned mainly with the mechanisms involved in foam propagation in porous media (which are embodied primarily in recent work), some literature has been purposely omitted. The reader is encouraged to review Marsden's work for further insights. In addition, the merits of micromodel usage were paramount in importance. Consequently, a search concerning the variety and effectiveness of micromodels was conducted. A brief discussion of the contributing papers is provided.

Section 2.1

Mechanism of Foam Flow in Porous Media

Foam has been described as a dispersion of gas bubbles in liquid. Bordering gas bubbles are thin liquid films called lamellae. Bikerman (1973) suggests that these surfactant stabilized films be treated as mathematical surfaces with thicknesses on the order of 10-100 nm. In order to create foam, surface active chemicals are dissolved in the liquid and finally mixed with air. Outside the reservoir, because of the high interfacial

areas existing between the two phases, it is known that foams are thermodynamically unstable and eventually break forming larger bubbles. This breakage rate is a function of pressure, temperature, and "surfactant" concentration. Foam propagation in porous media is of primary concern since that is where foam's application lies, and capillary pressures can conceivably affect the breaking of bubbles into larger ones and inhibit the production of multiple phases (including oil if present). This area will be discussed after a brief section on gas mobility in the presence of foam.

Section 2.1.1

Gas Mobility in the Presence of Foam

Before reviewing observed mechanisms of foam propagation in porous media, it is necessary to mention certain physical factors which can affect gas mobility considerably. As a reduction in this mobility is an objective in thermal recovery operations, knowledge of the pore blockage ability of foams is important. Pore diameter, surfactant concentration, and fluid flow rates can have an affect on observed phenomena.

Bernard and Holm (1964) showed that greater gas mobility reduction took place in high permeability sands rather than in lower ones. This realization occurred to Raza (1970) as well, who further stated that these high permeability sands possessed uniformly distributed large pores in which to generate large, high quality bubbles typically of at least a pore or two in size. Mast (1972) discussed this important relationship of pore geometry to bubble formation and derived equations linking bubble radius with pore dimensions. This factor is still very much considered as Hirasaki (1987), and Persoff (1991) regard bubble texture (bubble size and distribution) to be the most crucial factor controlling foam flow.

One of the most important physical descriptors of foam is a ratio termed foam quality. It exposes the relative amount of gas and liquid contained within the foam. Works by Holm (1968), David and Marsden (1969), Raza (1970), and Mast (1972)

demonstrate that surfactant concentration affects foam quality and size. It was found, by Mast, that lower, more dilute concentrations of surfactant led to "coarse" foams. Further, high active weight concentrations caused fine grained, stable foams and allowed the creation of bubbles strong enough to pass through pore throats without breaking. This creation allows for improved propagation in the reservoir, and the occupation of more liquid filled pores. Indeed, Holcomb et al (1981) and Huh et al (1988) indicate higher sweep efficiencies occur with higher foamer concentrations. Holcomb et al suggests that efficiency improvement continues until the critical micelle concentration is reached. At such time gas mobility flattens.

Various studies have also suggested that the foam has smaller bubbles at higher flow rates which leads to a greater reduction in mobility and improved sweep (Treinen et al. 1985: Owete et al. 1986: and Huh et al, 1988).

As mentioned already, these factors can be considerable, and the list itself may be incomplete. Injection procedures and pore surface wettabilities can also contribute to gas mobility effects. Clearly then, it is important to minimize or isolate mobility variables so that an understanding of mechanisms can be gained. Mechanisms of foam propagation can now be considered.

Section 2.1.2

Propagation of Foam in Porous Media - Early Work

Early work by Fried (1961), Bernard and Holm (1964), Kolb (1964), Marsden and Khan (1966), Raza and Marsden (1967), Holm (1968), David and Marsden (1969), Nahid (1971), and Mast (1972) each described the apparent pseudoplastic, high viscosity behavior of foam. Their descriptions of foam undoubtedly supported further application of it to petroleum interests. Due to certain physical limitations, however (the primary one being an inability to see through rock to observe flow, another one dealing with the inability to accurately replicate heterogeneity observed in porous media), uniformity of

opinion on theory describing foam flow mechanisms was much less apparent. Three popular mechanisms mentioned were homogenous fluid flow, pore channel flow, and "breaking and reforming."

The *homogenous fluid flow* mechanism theory was introduced and supported by researchers such as Fried (1961), Marsden and Khan (1966), Raza and Marsden (1967), and David and Marsden (1969). The main thrust of the theory is that foam is considered a continuum, behaving as a single fluid of high apparent viscosity, with gas and liquid flowing at the same rate. This idea was not extremely complex and made computations easier. Raza (1970), however, considered the homogenous fluid flow mechanism - and rejected it, arguing that foam injectivity didn't match that of high viscosity oil. One single viscous fluid, he reasoned, couldn't adequately describe the results.

Contrary to the notion of a continuum, Holm (1968) stated his belief that foam is continually reformed in porous media, repeatedly separating into gas and liquid phases. This belief supported *pore channel flow* theory where various phases are said to flow through separate pore throats, and permeability was a function of saturation alone. Again, work by Raza (1970) amongst others disproved the notion that the permeability of foam was solely saturation dependent.

Conclusions by Fried (1961), Bernard et al. (1965), Holm (1968), and Mast (1972) have lead directly to theories still in vogue today. Individually, they proposed that the gas phase flowed through porous media by *breaking and reforming* foam bubbles. They believed that the gas phase is discontinuous and at times is trapped, while the liquid phase travels freely through the connected film network. Further, Nahid (1971) advanced thought on this mechanism by showing that this fluid flow can be considered Darcy flow once a correction factor for gas permeability was used. He also showed that an immobile gas saturation existed, through the use of tracers. His findings revealed increased immobile gas saturation with increased surfactant concentration, highlighting the important effects of foamer concentration and propelling us into current research.

Section 2.1.3

Propagation of Foam in Porous Media - Current Work

Marsden (1986) and Owete et al. (1986) reiterated these findings concerning early foam work, surmising that gas viscosity was indeed a function of the gas flow rate, flow history and surfactant concentration, and that "breaking and reforming" processes is a dominant mode of foam propagation in micromodels. Sanchez and Schechter (1986), using simplified capillary tube models, went on to suggest that gas permeability was a function of wetting phase film thickness. Collectively, their works also signal the advent of current research. as a consensus of opinion concerning these "breaking and reforming" processes as dominant mechanisms of propagation has taken hold.

Homogeneous and heterogeneous models were used by Owete et al. (1986) to observe foam flow mechanisms. They found that flow mechanisms varied greatly between model types. Flow in the homogeneous model is described as *modified channel flow* in which air flows through channel pores defined by a network of liquid films. Breaking and reforming of foam bubbles was not observed, as interfaces deformed to pore geometry rather than break. In the heterogeneous model, they noticed foam bubbles were produced at pore necks to adjoining pores supporting breaking and reforming processes.

Using monodisperse homogeneous bead packs, Radke and Ransohoff (1986) described three foam generation mechanisms - lamella leave behind, gas bubble snap-off, and lamella division. Their work suggested the existence of a "critical velocity" above which strong foams develop, and below which a weak foam is formed. They credit Mast (1972) for being one of the first to attempt an understanding of foam generation mechanisms through visual observations, and argue that because these three mechanisms were observed, in parts, in other porous media (Owete et al., 1986; Mahmood and Brigham. 1987; Huh et al., 1988; Hanssen and Jacobsen, 1989) "they are relevant to all

types of porous media." "Snap-off" was already a part of foam vocabulary. With their work, "leave behind" and "division" were instantly accepted as descriptive terms of foam flow mechanisms.

Lamella leave behind, the dominant generation mechanism below the critical velocity in bead packs, occurs when two gas bubbles invade the same pore body from different directions. The liquid in the pore space is squeezed into a lamella by the two advancing fronts. This squeezing process likely fills in pore bodies initially passed by the leading foam front and allows for continued overall advancement. Dead end pathways are created by lamellae blocking pore flow channels thereby reducing relative permeability to the gas phase.

Radke and Ransohoff (1986) point out that only a moderate increase in resistance to gas flow was experienced with leave behind, and that it, consequently, provides weak foams. They also state that it provides for the generation of a lamella alone, and the source potential for flowing lamellae. No separate gas bubbles are formed in this process. Should the lamella rupture, they offer, complete liquid saturation of the pore is necessary for another lamella to form.

Snap-off mechanisms involve the actual breaking of an air bubble into another discontinuous bubble, and seems to occur at narrow pore throats. At low capillary pressures a "collar" of water accumulates around a continuous air bubble in a pore throat. As capillary pressure decreases, this collar thickens until it bridges the throat, blocking air flow, and leading to the eventual creation of a new lamella. As Rossen (1995, unpublished) mentions, an interesting aspect of snap-off is that the capillary pressure below which snap-off occurs is actually lower than the capillary pressure above which gas would displace liquid filling the same throat. As air must first enter the pore body before disconnection, fluctuating capillary pressures are a necessary ingredient to snap-off.

Snap-off is believed to be the predominant foam generation mechanism. New

bubbles are created repeatedly by snap-off from the same site, making snap-off a major contribution to gas flow resistance, creating lamellae and strong foams. Roof (1970) and Mohanty et al. (1980) each studied and reported specific pore geometries necessary for snap-off mechanisms. Roof noted that "the front (head meniscus) is always at least seven pore radii from the throat of the constriction before snap-off can occur." Mohanty et al. calculated that snap-off occurs when the ratio of pore body radius to adjacent throat radius exceeds three.

Lamella division is described by Radke and Ransohoff (1986) as a secondary generation mechanism as it requires the movement of lamellae before it can actually occur. As the moving lamella approaches a pore body containing more than one other throat, it can either choose one throat - usually the path of least resistance - or it can split occupying several pore throats and creating new lamellae. Like snap-off, this mechanism creates new air bubbles which can impede further air flow, and can occur repeatedly at the same site.

Lamella leave behind, lamella division, and snap-off are the three mechanisms by which foam is generated in a porous medium. In steady state the rate of generation must be equal to the rate of collapse of lamellae. This is the essence of the population balance approach proposed by Falls et al. (1988), and Kovscek et al. (1994).

Lamellae are destroyed by two processes. The first is when a lamella thins and breaks - the lamellae are thermodynamically metastable and so will collapse by drainage of water out of the film. The second process is coalescence of lamellae. This is when two lamellae are separated by a small gas bubble which is at a higher pressure than the gas on the other side of the lamellae. By diffusion the gas leaves the small bubble and the two lamellae come together.

Castanier and Hanssen (1995, unpublished) noticed the sliding of lamellae (bubble train flow) over liquid films covering the grains in silicon micromodels exactly like the ones used in this project. Using atomic force microscopy to investigate the

liquid/solid interface, a thick layer of surfactant (60 nm in diameter) was found. This layer, they state, could explain the apparent bubble train affect observed.

Section 2.1.4

Effects of Oil on Foam Propagation

The previous mechanisms described involve experiments which excluded any presence of oil in the porous medium. An argument for leaving out oil is simply that a need to understand the basic propagation mechanism dictates such a move. Any additional components only serve to complicate matters. That an oil phase alters observed processes was suggested by Nikolov et al (1986). When studying bulk foam/oil interactions, they reported the possible occurrence of three distinct films during the process of three phase foam thinning. They are foam films, which are water films between air bubbles; emulsion films, which represent water film between oil droplets; and pseudo-emulsion films where water film resides between air and oil droplets. Nikolov et al pointed out what was termed a "destabilizing effect" of crude oil on foam, noting that surfactant type and concentration influenced emulsion structure stability. Their findings that pseudo-emulsion films, droplet size, and droplet number may all contribute to foam destabilization was supported by the works of Manlowe and Radke (1990), Schramm and Novosad (1990), and Schramm (1992).

Further insight into the effects of oil saturation on foam propagation was provided by Lau and O'Brien (1988). Their work relies upon an understanding of oil spreading ability (Ross, 1950), in which spreading is determined from "spreading coefficients" or free surface energies. Interfacial tension of the various phases in contact with each other are combined (gas/oil and oil/water tensions are subtracted from gas/water interfacial tension) to provide a spreading coefficient. If the coefficient is positive, then spreading of oil between the gas/water interface occurs. If negative, then no spreading occurs, and no destabilization occurs. Through the use of sandpacks and both spreading and

nonspreading oils, they were able to show an increase in foam generation time, a reduction in foam propagation rate, and an increased foam destruction rate with spreading oils. These results all pointed towards oil invasion into aqueous surfactant/air boundaries. This finding is, however, contrary to Manlowe and Radke's who argue that there is no correlation between oil spreading and foam stability. Instead, they state pseudo-emulsion film collapse is the general destabilization mechanism.

Other explorations into oil saturation effects centers around reservoir wettabilities. Huh et al. (1988) found that micromodel wettability was altered to intermediate or oil-wet as a result of crude oil saturation. The effects of various phase affinities to grain surfaces was studied by Sanchez and Hazlett (1989) as well. They performed water-wet and oil-wet experiments using glass beadpacks, finding no difference in gas permeability reduction for similar surfactant concentrations. An indication of surface reaction, from hydrophobic to hydrophilic, was detected, however, after the addition of surfactant. This fact, along with a shift in liquid phase relative permeability of the oil-wet medium suggested to them wettability alteration. Kuhlman (1990) commented on similar results of his own, remarking that the deleterious effect of oil on foam was due in part, at least, to the high concentration of light hydrocarbons in the oil, and the oil wetness of the porous medium itself. Work by Hornbrook et al. (1992) noted that wettability alteration was due to the surfactant injection procedure. They found with slug surfactant injection, oil appeared to be the wetting phase, and with foam injection, surfactant appeared to wet the medium. Clearly, more work in this area is required.

Section 2.2

Micromodels

The use of micromodels as a tool for understanding pore level processes has existed for quite some time. Throughout this literature review, different micromodels

provided substance to theories expoused by their authors. Such micromodels include simple capillary tubes (Marsden and Khan, 1966 and Sanchez and Schechter, 1986), glass beadpack which can be homogeneous or heterogeneous (Sharma, 1965 and Radke and Ransohoff, 1986), etched glass (Mattax and Kyte, 1961, Davis and Jones, 1968 and Mast, 1972), etched plastic (Bonnet, 1978), and etched silicon (Owete and Brigham, 1986 and Hornbrook et al. 1992). All of these models provided valued insights, the merits of which can and has been debated.

The variety of micromodels employed for studies however, suggests an underlying problem with their usage. The objective of micromodels, and any other type of model for that matter, is to replicate the features of the medium it represents. Reservoirs are three dimensional and heterogeneous by rule. As Sarathi (1986) points out, micromodels in general suffer from several distinct limitations. They are a difficulty in obtaining a specific etch depth necessary for the sake of heterogeneity; the unintentional introduction of microscopic heterogeneities into the model through the etching processes themselves; the fact that two dimensional micromodels required for visualization cannot ever demonstrate the continuity with multiple phases that three dimensional models permit; that Peclet numbers, defined as the ratio of convective to dispersive transport, are altered due to pores in micromodels generally being larger than true reservoir pores; and finally, differing pore structures from reservoirs due to an inability to capture rock characteristics such as heterogeneity, pore geometry and wettability. Their usage, Sarathi reasoned, should always be done with these limitations in mind.

Owete and Brigham (1986) and Hornbrook et al. (1992) employed the use of silicon micromodels to study foam propagation. Due to a novel fabrication technique, these models were able to rule out all of the concerns of Sarathi (1986) except for the loss of three dimensional continuity. The generally accepted success of this technique is the justification for their employment (with certain modifications) in my research. As the micromodel construction will be described in Section 4, further descriptions will be

omitted at this time. A discussion of the experimental apparatus (Section 3) precedes it.

Section 3.
EXPERIMENTAL APPARATUS

In order to evaluate fully the pore level interactions occurring in the micromodel, it was imperative to employ both visual and indirect means to gather supporting data. Consequently, three systems were developed to work in concert with each other - the fluid flow system, the direct observation system, and the pressure measurement system. Several pieces of equipment have been acquired and used expressly to support these systems. The systems and their respective components will be described in this section. The experimental set-up is shown schematically in Figure 3.1.

Section 3.1

Fluid Flow System

After initial flooding of the micromodel with measured aqueous surfactant solution from a vacuumed state, all other fluids enter the medium through a syringe pump. The fluid flow system, then, is composed of a syringe, a syringe pump, a micromodel, a graduated cylinder, and connecting tubing.

A Becton-Dickinson syringe, filled with the required fluid is firmly placed on the syringe pump stage. The syringe pump, Sage Instrument's Model 355, is composed of

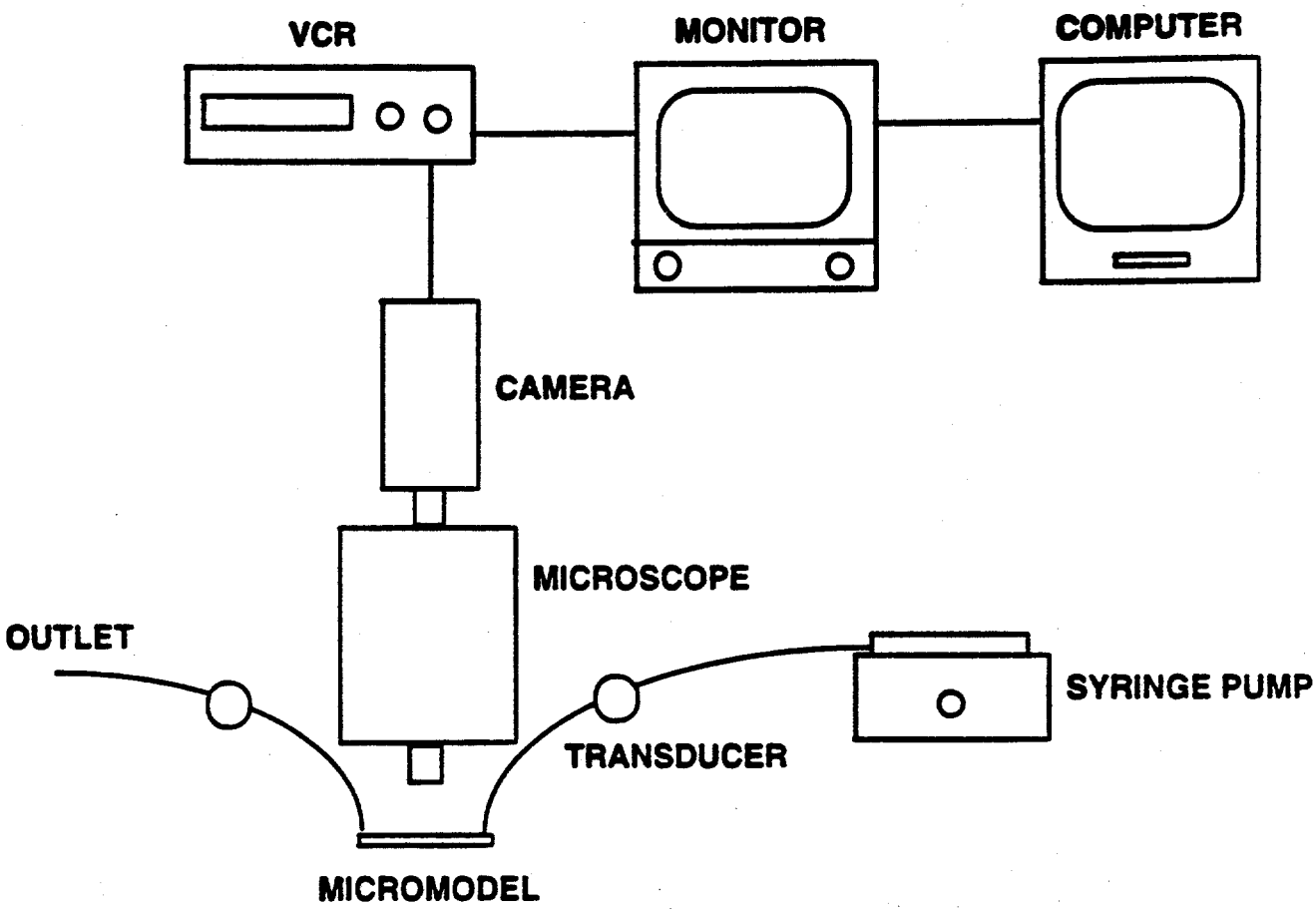

Figure 3.1 Experimental apparatus schematic.

synchronous motors which, when engaged with the carriage on the stage, depresses the syringe plunger at a constant rate. Nominal displacement rates, calculated by the manufacturer, are available for this pump for a variety of syringe sizes. This model also gives one the ability to vary the percentage of flow, further enabling flow rate variation and control. Consideration for the inclusion of incompressible fluid flow rates has been given. This calculation procedure is found in Section 5, after the discussion of the silicon micromodel (Section 4).

Section 3.2

Direct Observation System

As can be deduced from its title, the direct observation system was designed to provide visualization of pore level displacement events. Viewing such events, it is possible to measure pore diameters, bubble sizes, contact angles, etc., and gain insights from their relationships. The system, therefore, is composed of a microscope, a video camera, a video cassette recorder, a television monitor, and a computer.

The Nikon Optiphot-M microscope allows for dual viewing of the micromodel from the attached binoculars or through video imaging via the provided phototube. Reflected light (12 volt / 50 watt halogen) necessary for silicon micromodel work, is split from its source to provide this option. Two objectives, 5X and ELWD 40X (working distances of 20.0 and 10.1 mm, respectively), are attached to the revolving nosepiece and allow for microscope stage movement without its motion affecting the micromodel or its ports. Approximate view field diameters seen from the two objectives are 3,000 microns with the 5X, and 390 microns with the ELWD 40X. Features a micron in length can easily be seen with the ELWD 40X objective.

The video camera used is a Sanyo closed circuit television camera. A universal microscope adapter enables attachment to the microscope, with image viewing made possible via the previously mentioned phototube. This image is recorded on a Mitsubishi

high resolution videocassette recorder at a rate of thirty frames per second. After recording, the displacement events can be played back, frame by frame, for detailed analysis. A Sony, high definition color monitor assists in this analysis.

Finally, an image can be sent to the attached Macintosh computer for further analysis. Public domain image processing software (*Image* version 1.43, by Wayne Rasband, National Institute of Health Research Services Branch, NIMH) allows for the capture, enhancement, and printing of the desired image.

Section 3.3

Pressure Measurement System

As the direct observation system involves the viewing of pore level events, the pressure measurement system requires the reading of relative drops in pressure as indirect evidence of these multiphase interactions. The system is composed of pressure transducers, demodulators, and a data logger.

Two Celesco differential pressure transducers are used to measure inlet and outlet pressures during experimentation. Positive leads are opened to atmosphere, while the negative ones are connected to pressure ports. Two twenty-five psi pressure plates are attached to the transducers. Pressures significantly higher than twenty-five psi dramatically test the micromodel's strength as currently designed.

Electrical signals generated at the pressure transducers are sent to Celesco carrier demodulators. These demodulators convert fluctuating voltages into psi values. The values are transferred into graphical form by a Soltec data logger. The logger plots inlet and outlet pressure next to each other versus chart recording speed.

With the incorporation of both visual and indirect observations a better understanding of the displacement events is gained. These benefits will be discussed in later sections. The next section deals with a major benefit to this work - the silicon micromodel.

Section 4.
THE SILICON MICROMODEL

Previous research has shown that different types of micromodels can produce results which cannot be matched in micromodels composed of other materials, or etched in another fashion. Indeed, as mentioned already in the literature review, Sarathi (1986) discussed the unintentional introduction of microscopic heterogeneities through the etching process, differing pore structures from true reservoirs due to an inability to capture rock characteristics (heterogeneity, pore geometry, wettability, etc.), and the loss of three dimensional continuity, amongst others. A novel micromodel fabrication technique has been pioneered at Stanford (Owete and Brigham, 1986; Hornbrook et al., 1991,1992) which eliminates virtually every concern of Sarathi's except for three dimensional continuity. It should be noted, however, that even this objection was considered in Hornbook's design, as three dimensional connectivity characteristics were "sculpted" into the micromodel by computer. This model is composed of silicon, and its pattern replicates that of Berea Sandstone.

Five heterogeneous micromodels were constructed for this project. All of these models employed are exact duplicates of each other. A detailed description of the fabrication of the models can be found in Hornbrook et al. (1992). This section contains a summary of micromodel construction, description of its pore structure, and fluid flow analysis.

Section 4.1

Micromodel Construction

The micromodel employed is made of silicon. A detailed heterogeneous network is etched onto the silicon wafer. In order to get to the point of etching, and to complete micromodel construction, a series of steps are required - imaging, etching, bonding, and finishing. The manufacturing process is shown schematically in Figure 4.1.1.

Imaging of the model onto the silicon wafer involves the digitization of a rock section into a computer from a high quality photograph. The section, which is approximately 500 μm across, is replicated many times to fill an area 5 cm squared. Assurance of two dimensional connectivity is made, and this image is reproduced as a chrome on glass mask. The grains are now opaque and the pores are transparent. A coating of photoresist is placed on a silicon wafer. As ultraviolet light kills photoresist, it is shined through the mask onto the wafer. After exposure, the flow path image exists as clean silicon for the pores and photoresist coated silicon for the grains.

Using the pattern provided by the photoresist, a dry etch technique is used to create the network of pores and grains in the wafer. As the micromodel is an exact replica of Berea sandstone in two dimensions, this is not true in its third dimension - etch depth. Since exact duplication of three dimensional flow is impossible for direct visualization purposes, a uniform etch depth is made throughout the micromodel. Owete and Brigham (1986), and Hornbrook et al. (1991, 1992) both used an etch depth of 5 μm. It is, however, possible to etch to a depth of 30 μm without the loss of detail. The micromodels used in this project were etched to 15 μm. It should be noted that variation in etch depth can cause permeability changes from the rock it models and previously constructed micromodels. This effect cannot be avoided. Further, the ability to alter permeability should be considered an asset.

Bonding, anodically, requires the placing of a glass plate (Corning Pyrex #7740)

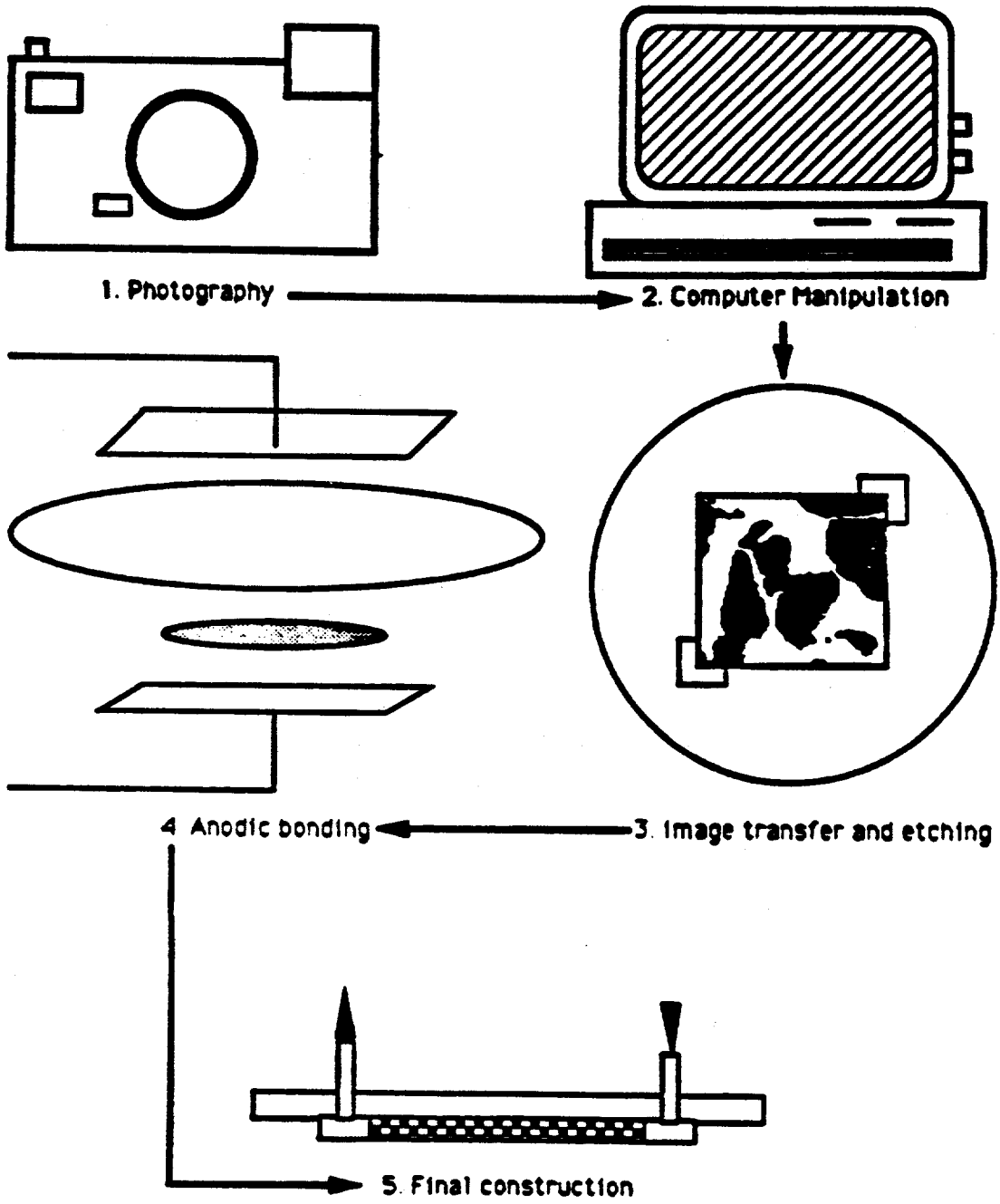

Figure 4.1.1. Step-by-step model construction.

atop the etched silicon wafer. Port holes are drilled and aligned to match those on the sterilized wafer. Electrodes are attached to the model, and the entire assemblage is heated to a temperature above 200 °C. A 600 volt potential is applied to the electrodes and bonding occurs.

After bonding Swagelock ports were attached to the drilled holes in the glass through the use of a high strength epoxy (Miller-Stephenson Epoxy 907). An additional glass plate was epoxied to the wafer's bottom to provide added support. A description of the model's pore structure follows.

Section 4.2

Micromodel Pore Structure

Figure 4.2.1 schematically reveals the fluid flow area of the micromodel. It is composed of an inlet, the pore network, and an outlet. The inlet and outlet provide the opportunity of invasion and exit of fluids from multiple pore throats. As this is a heterogeneous model pore widths vary both randomly, and two dimensionally. The flat glass roofing and the constant etch depth allow for the exact geometrical description of any pore. Figures 4.2.2 and 4.2.3, courtesy of Rogaland Research, are S.E.M. examinations of the micromodel pore structure used in this project. Black objects represent the grains, white outlinings are the grain walls, and the gray pattern is the pore space. The reader should also note the lack of angularity which is often introduced during etching processes.

Within Figure 4.2.2, the smallest pore pattern, approximately 500 μm squared can be observed. Overall pore connectivity, dead end pores, and irregular pore sizes which affect air/liquid displacements can also be seen, demonstrating the model's heterogeneity. An analysis of fluid flow characteristics follows.

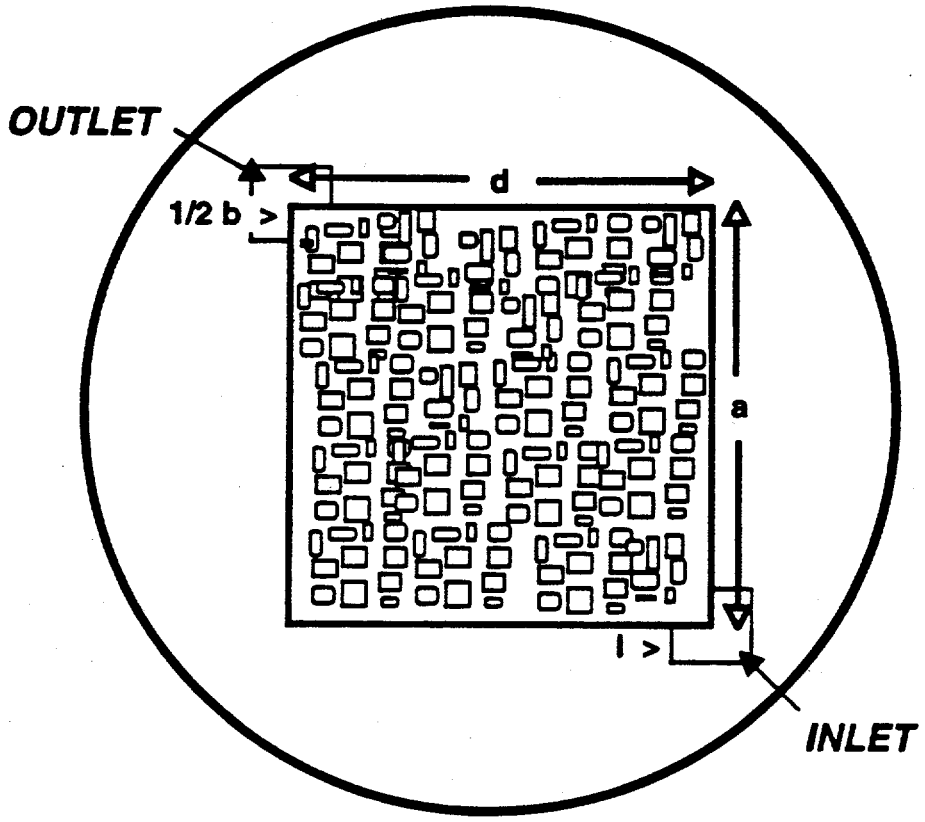

Figure 4.2.1 Schematic of micromodel fluid flow area.

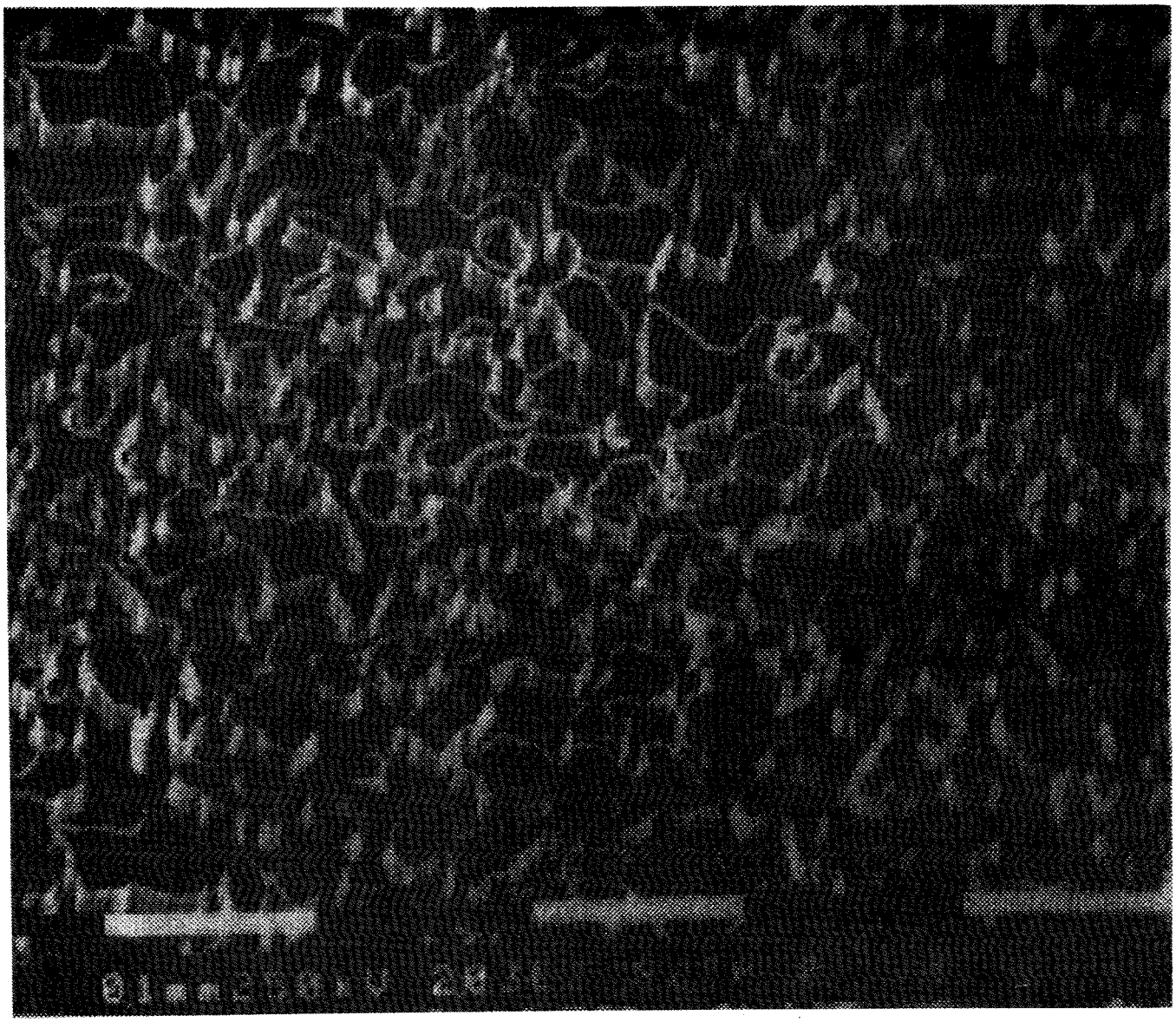

Figure 4.2.2. SEM view of the whole pattern.

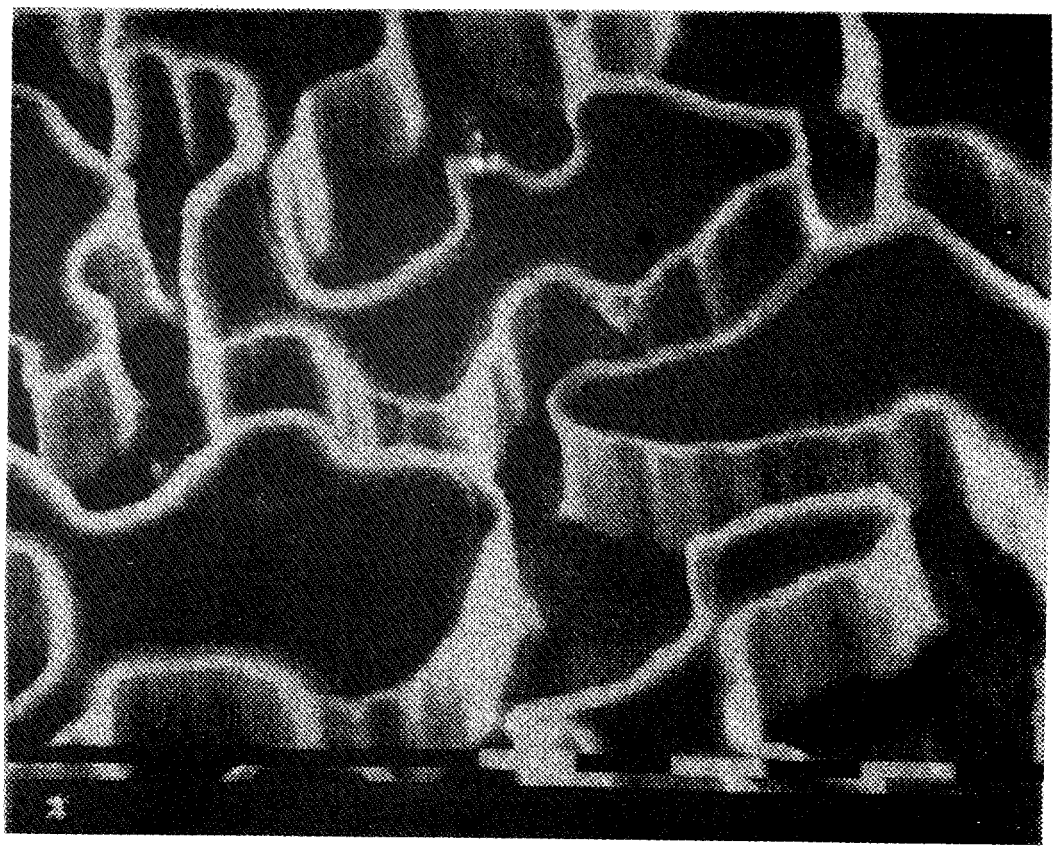

Figure 4.2.3. Detailed SEM view.

Section 4.3

Micromodel Permeability Calculations

The model geometry is one-quarter of a five spot with injection and production wells located inside square open ports as shown below. The problem consists of calculating the pressure drops caused by the empty squares around the wells and calculating the effect of the five spot geometry for the remainder of the model.

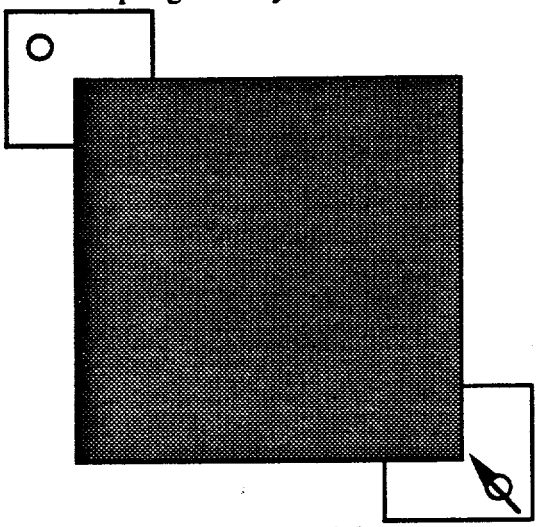

Figure 4.3.1 Micromodel geometry.

Section 4.3.1

Treatment of the Well Inside the Empty Square Slot:

The real geometry of an empty slot is presented below;

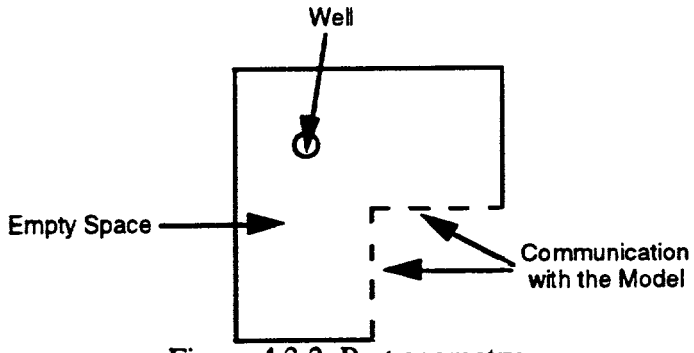

Figure 4.3.2 Port geometry.

This system can be roughly approximated at steady state by the system shown below, with a well in the center of a squarewith an open side.

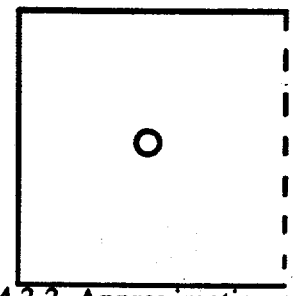

Figure 4.3.3 Approximation of a port.

The shape factor for such a system can be estimated from the data of Ramey et al. (1975) (or from Fig. C.21 in Earlougher's monograph, 1977). For long times (steady state flow) the dimensionless pressure is equal to 8.904.

The numbers are as follows for the model used in the experiments:

Well radius, 1mm

Square side, 5mm

Depth of the empty space, 20 microns

Flow rate of liquid, 1cc/min

Liquid viscosity, 1cp

Neglecting two phase effects and using these numbers we find a difference in pressure between the well and the constant pressure boundary of 1×10^{-6}psi. This is negligible for all practical purposes. Of course, the geometry of the open square is not the same as the actual system, but it is clear that it would predict a greater pressure drop than the actual geometry.

Section 4.3.2

Five Spot Geometry

The system can now be evaluated as a quarter of a five spot with two injectors and two producers located in the middles of the linear contacts between the porous medium and the empty squares. A schematic of the system is given on the next page.

To define the pressure drop across this setup, one must treat it as a quarter of a five spot. It is then necessary to desuperimpose the doublet part of the quarter of the five spot and replace it by the two injector two producer system (Chen and Brigham, 1974). This concept is shown in the next figure:

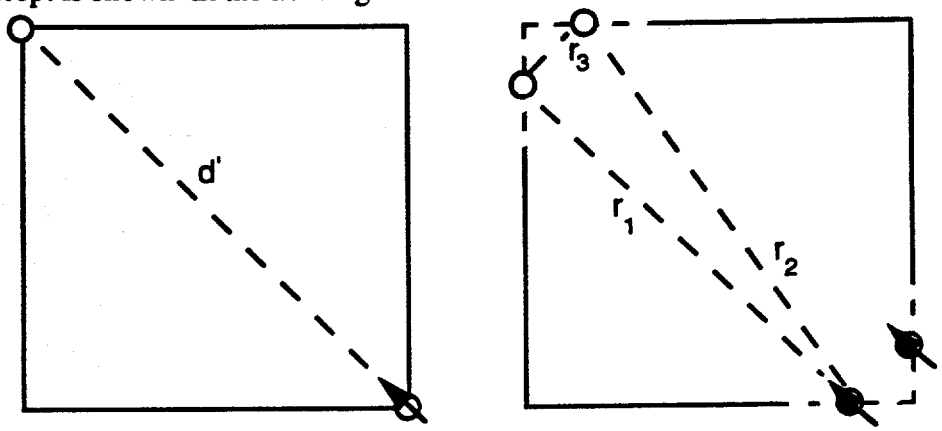

Figure 4.3.4 Desuperposition from five-spot to model geometry.

The equation for the five spot is given as:

$$\Delta p = \frac{q\mu}{\pi kh}\left[\ln\left(\frac{d'}{r_w}\right) - 0.619\right] \tag{4.1}$$

where d' = The distance between injector and producer.

This is Eq. 6.43 from Craft and Hawkins. Note that their constant, 3.54, is wrong and should be π in Darcy units (Brigham, Injectivity, class notes for P.E. 270A).

The equation for the pressure drop across a doublet is given by:

$$\Delta p = \frac{q\mu}{\pi kh}\ln\left(\frac{d'}{r_w}\right) \tag{4.2}$$

The four wells in the constant pressure system have an equivalent well radii of one-quarter of their constant pressure segment lengths. Using the distances defined in Fig. 4.3.4, one can calculate the pressure drop between injectors and producers. This is given by:

$$\Delta p = \frac{q\mu}{2\pi kh}\ln\left(\frac{r_1 r_2}{r_3 r_w}\right) \tag{4.3}$$

This equation is derived using the concepts in Brigham's doublet notes (class notes for P.E. 224). The final equation for the pressure drop across the micromodel can now be

written as:

$$\Delta p_{5spot} - \Delta p_{doublet} + \Delta p_{4wells} = \frac{4q\mu}{\pi kh}\left[\frac{1}{2}\ln\left(\frac{r_1 r_2}{r_3 r_w}\right) - 0.619\right] \qquad (4.4)$$

Note that the Eq.4.4 has been multiplied by four to take into account the fact that the model is only one-quarter of a five spot. An interesting fact is that the equivalent wellbore radii are very nearly equal to the geometric average of the distances between adjacent wells and their radii.

Section 5.

EXPERIMENTAL PROCEDURE AND FLOW CALCULATIONS

Hornbrook et al. (1992) described the complex interaction of crude oil with surfactant. As a result of the strong effects observed by Hornbrook, coupled with the findings of concentrational effects on gas viscosity, it was determined that smaller surfactant concentrations and basic mineral oils should be used for preliminary study.

In order to create a basis from which to compare oil/surfactant/air results, water/air and surfactant/air experiments were performed. The surfactant, AOS 1618, was chosen since it was used prominently in prior research conducted at SUPRI. This Shell Development Company product, as designed, should be suitable for both heavy and light oil experiments, and is characterized as being spreading conducive. Surfactant concentrations were determined from the known percent by weight of surface active material contained within the bottled surfactant solution. Consequently, AOS 1618 concentrations of 0.001% by active weight, and 0.01% by active weight were used in the two phase runs. The aqueous solution serves as the liquid phase, and air serves as the gas phase.

The two phase work completed, three phase runs containing a residual oil component were accomplished . In each run, decane represented the oil phase, and the surfactant concentration remained at 0.01% by active weight. The type of surfactant

varied though, from the spreading conducive AOS 1618 to the spreading inhibitive B1333, in an attempt to better understand foam propagation complexities. All experiments were performed at room temperature. The following is an explanation of the experimental procedure and results calculations.

Section 5.1

Experimental Procedure

To ensure relevance of results, experimental procedures were followed in the same manner in each case. Prior to each run the micromodel is vacuumed, and the various components of the experimental apparatus recalibrated. The vacuum on the micromodel and plumbing is broken upon exposure to a column of deionized water, or an aqueous solution of deionized water and surfactant. As a result of exposure, the micromodel, almost instantly, is completely saturated with fluid. Visual observation of the pores confirms saturation. Several pore volumes of air is drawn into a B/D syringe and the syringe attached to the pump. The outlet is then opened to atmosphere, and the experiment is ready to begin. The constant rate injection pump is activated and pressure buildup starts. During experimentation, displacement events are viewed and recorded. Once breakthrough occurs, pressure drops significantly, and no more fluid is produced, the experiment is terminated.

Oil phase procedures differ slightly from the description above. For three phase work, procedures detailed by Manlowe and Radke (1990) were adopted. In short, the micromodel is saturated with an aqueous surfactant; then flooded with oil up to a pressure of approximately 18 psig; reimbibed with surfactant until no more oil is produced, leaving a residual oil saturation of approximately 35%; and finally drained by air injection. This mimics gas injection into a residual oil and aqueous surfactant solution. Pressure and visual data are then ready for analysis.

Section 5.2

Air Mobility Calculation Procedure

Air was injected into the micromodel at a constant pump rate to displace liquid. As a result of air displacement, the pressure drop, (Δp), across the model was graphically monitored as a function of time for each experiment. The use of this data, along with the known micromodel dimensions, allows the ability to perform air mobility calculations.

Owete et al. (1984) devised a method of calculating effective air mobility. Their method will be adopted here. The reader is encouraged to review their paper for a detailed description of the calculations involved. In short, the actual air flowrate at the inlet end of the model is:

$$q_a = R\left(1 + \frac{\Delta p}{p_a}\right) + \frac{R t - V_s}{p_a}\left(\frac{d(\Delta p)}{dt}\right)$$

where:

q_a=actual flow rate, cc/s

R=syringe pump rate, cc/s

V_s=initial volume of air in syringe, cc

t=time,s

The average pore pressure over the desired time interval can be calculated from the known average inlet and outlet pressures. It is :

$$\bar{p} = \frac{\bar{p}_1^2 + p_a^2}{2 p_a}$$

where:

$\bar{p}$ = avg. pore pressure

p_a = atm. pressure

p_1 = avg. inlet pressure

The air flowrate measured at the average pore pressure is obtained by:

$$\bar{q} = \frac{p_a}{\bar{p}} (q_a)$$

And, effective air mobility, M, is calculated from:

$$M = \frac{\bar{q}}{\Delta p}$$

Section 6.
RESULTS

Experiments have been conducted to study foam flow with and without the presence of oil. Both pressure drop and visual information have been collected. These data (to be discussed in this section) are in the form of graphs, and videotapes, respectively, and are available at the Stanford University Petroleum Research Institute, Stanford, California. This section, then, will discuss the fluid flow mechanisms observed within the micromodels, the related pressure effects, and fluid flow calculations. Table 6.1 shows all experiment results, and Figure 6.1 provides pressure drop versus time-until-breakthrough results graphically for the same experiments.

Section 6.1

Fluid Propagation

As previously mentioned, a series of experimental runs were conducted without residual oil saturation. Surfactant and air interactions, then, comprised two phase experiments. Following them, decane was injected into the micromodel in the manner already described in Section 5.1. In every case, ten cubic centimeters of air was injected into the liquid filled model from a syringe. The pump injection rate used was 3.6E-4 cc/s. The runs differed from each other only in the amount of active surfactant concentration of

RUN	AVG. PRESSURE DROP psi	TIME TO BREAKTHROUGH s	AVG. FLOWRATE cc/s	EFFECTIVE AIR MOBILITY cc/s/psi	EFFECTIVE PERMEABILITY mD
WATER/AIR	6	19,080	0.0067	0.0011	26
0.001% AOS1618/AIR	9	22,320	0.0061	0.00068	17
0.01% AOS1618/AIR	19	28,080	0.0051	0.00027	6.4
0.01% AOS1618/ DECANE/AIR	6	67,680	0.0067	0.0011	26
0.01% B1333/ DECANE/AIR	7	69,840	0.0069	0.00099	23

Table 6.1. Silicon micromodel experimental results.

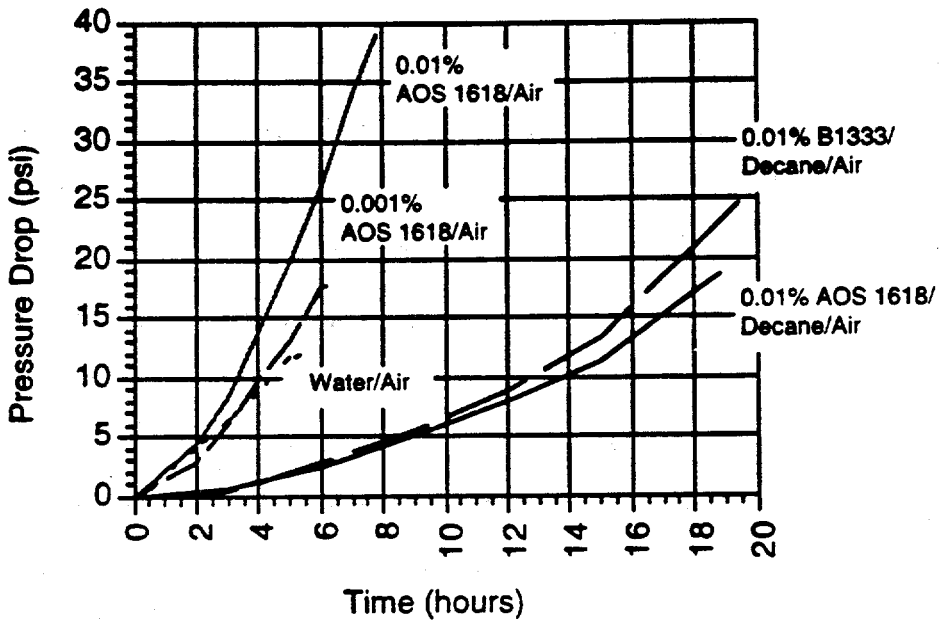

Figure 6.1. Time vs. Pressure in micromodel runs. The figure stops at breakthrough.

AOS 1618 contained within the liquid phase. Three runs were performed: with no surfactant, with 0.001% surfactant, and with 0.01% surfactant. The following is a discussion of observations made upon viewing the videotapes.

Section 6.1.1

Air/Water Interaction (No Surfactant)

Air flow resulting from deionized water and air introductions can be observed in Figure 6.1.1. This figure is a time progression of events occurring in the medium beginning with A and ending with E. The encircled dark regions are grains, the lightest is air, and the intermediate shade is water. Overall pressure drop occurs from right to left in this figure and others to follow. Wetting phase and individual phase determinations are made from radius of curvature observations. In this figure water is obviously the wetting phase, and is being drained by invading air. Flow represented by this figure occurs during a 6.5 minute interval, and is characterized by continuous air channels. The black arrows represent momentary flow directions. Within the pores, air follows a tortuous path to the outlet, splitting and reconnecting around grains, isolating water located in dead-end or circumvented pores, all without breaking and forming bubbles. No foam is created. Air at times occupied only a portion of the pore body in which it traveled.

At each stage in the displacement, the air passes through the largest available throat. This represents the throat with the lowest capillary entry pressure. The local configuration of the air is controlled by capillary rather than viscous forces. Notice that the local flow directions are not necessarily in the direction of the overall pressure gradient.

The pressure drop across the micromodel builds gradually to approximately 12 psi until breakthrough occurs. Pressure drops flatten to 10 psi afterwards, and decline upon the completion of 10 cc air injection.

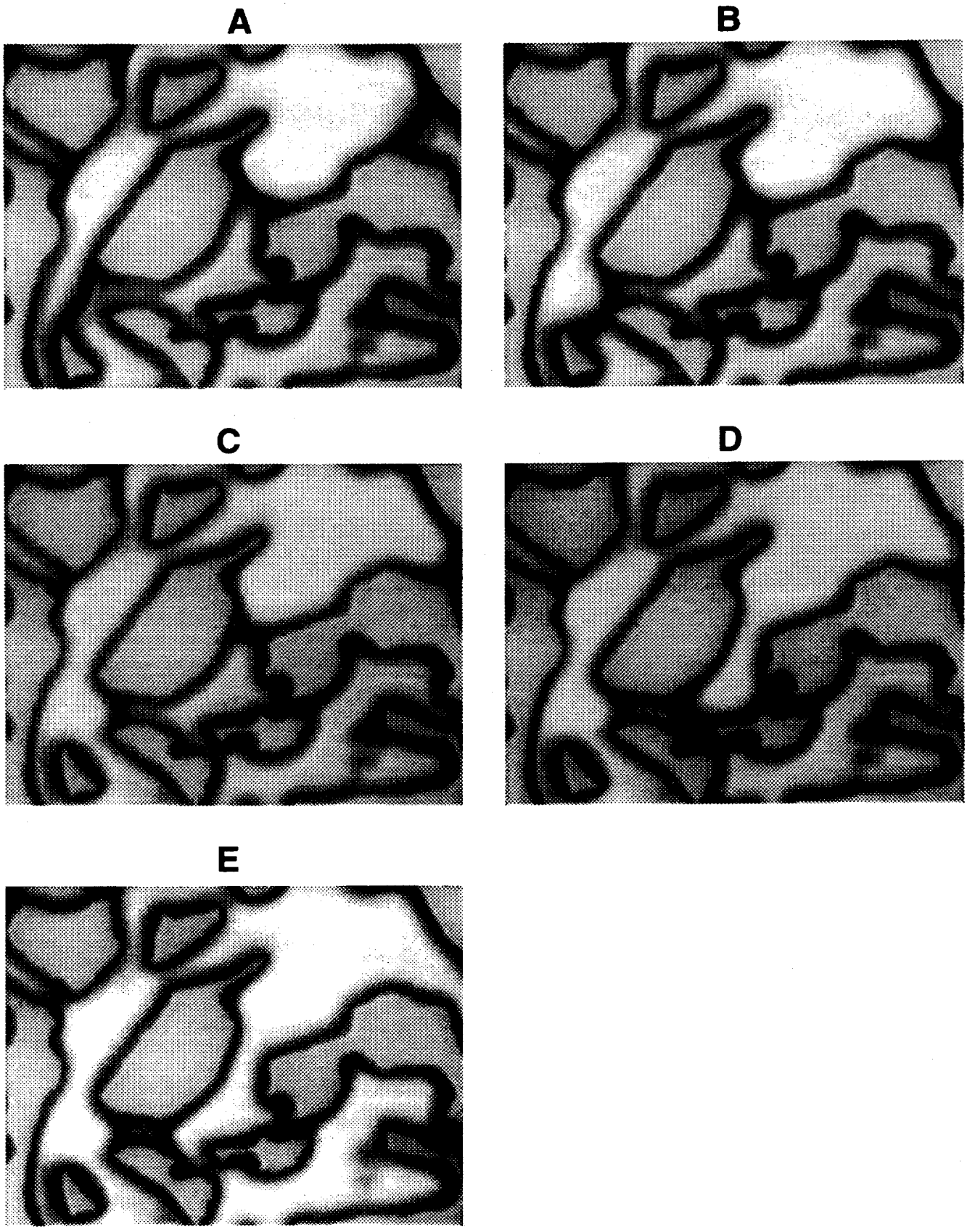

Figure 6.1.1 Air injected into water saturated micromodel.

Section 6.1.2

Air/AOS 1618

As previously mentioned, the two phase runs completed with surfactant were accomplished at concentrations of 0.001%, and 0.01% by active weight. Consequently, differing results were attained. Visually, the 0.001% active weight concentration was similar to the continuous air channel flow of the air/water runs. However, these channels became discontinuous after representing about a hundred pore lengths, and were called bubbles. The air was made discontinuous because of the presence of water filled throats rather than thin lamellae between the bubbles. The bubbles occupied the entirety of the pores in which they resided and were extremely stable. More of the micromodel itself was filled with air, suggesting deeper, more tortuous penetration. None of the propagation mechanisms described earlier in the literature survey (snap-off, leave-behind, and division) were viewed. Air moved through the medium by way of *modified bubble train flow* where bubbles traveled through pore throats and tended to reside more statically in larger pore bodies until enough force was applied to move them along. Again, no breaking and reforming processes were observed. The increase in tortuosity is confirmed by pressure readings which recorded an average drop of 18 psi across the micromodel.

With the 0.01% active weight concentration, air bubbles were on the order of two to three pore lengths as opposed to hundreds. Instead of painstakingly tracking flow paths to find bubble terminations, lead fronts and ends of most bubbles were visualized with little microscope stage movement. Like the lower concentration, the alternating advance/static motion of the bubbles at higher concentration supports modified bubble train flow. As with the comparison of the lower concentration to water, the higher concentration provides an even greater penetration within the micromodel. Stranded bubbles are viewed throughout the model. Unlike the lower concentration, however, some breaking and reforming processes are observed. Figure 6.1.2 presents one such breaking and reforming event. Again, a time interval approach is used to demonstrate

motion. Unfortunately, the speed at which these processes occur is more than 1/30th of a second. This leads to an inability to display the event in any more than a general sense. However, slides A through D clearly show air and water entering and leaving a pore throat in the left side of slide A. What we see here is air and surfactant alternately occupying a portion of the network. For most of the time the air/surfactant interfaces are located between pores and pore throats with the water residing in the narrowest throats. This is an extremely stable configuration. When air/surfactant interfaces straddle a wider pore, the interface moves rapidly to find a more stable location. This results in a stable foam, with few reforming and breaking events and few thin lamellae. Liquid flow along corners of the network and film flow across the grains allows the surfactant to reoccupy narrow throats that are filled with air, as seen in the sequence C to D.

This type of event occurred frequently in this location. However, the same pore design in other regions of the micromodel did not provide the same results. In some areas the pores were completely liquid filled. In others, air bubbles sat statically in pore bodies, exhibiting no movement at all. Moreover, after several minutes the breaking and reforming events died in this location as well. Most importantly, no snap-off events were observed.

Indirectly, a dramatically significant increase in pressure drop occurred with the surfactant dosage increase. Pressures up to 43 psig were recorded before breakthrough. A hummocky pressure pattern arose after breakthrough signifying the irregular nature of the surfactant ladened medium as pressures build and release in reponse to bubble trains entering and exiting thousands of pores.

Section 6.1.3

Air/Decane/AOS 1618

Before injecting air, the model possessed a residual oil saturation of about 35%. As seen directly, after injection, the air bubbles of this three phase run were distinctly

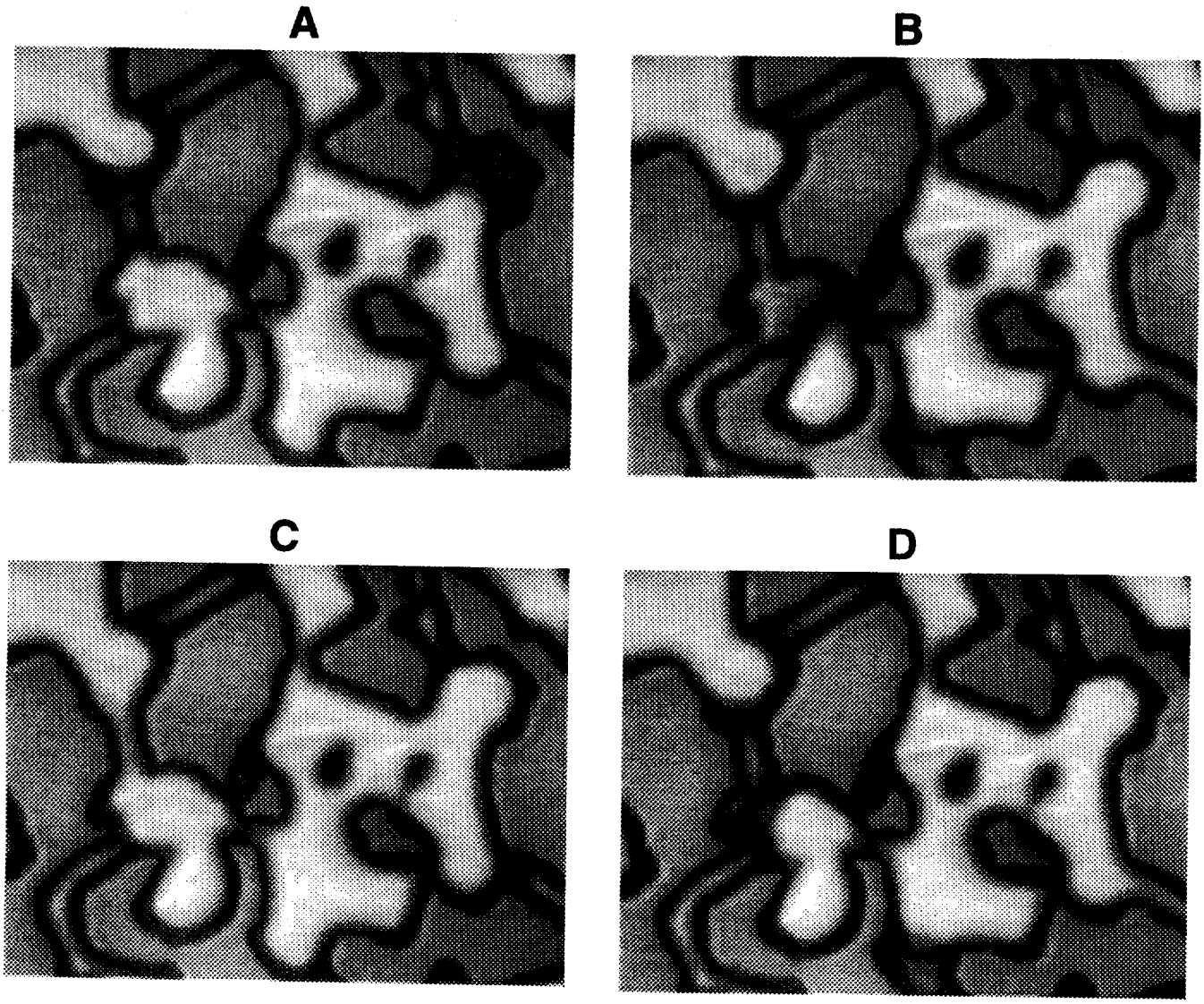

Figure 6.1.2 Air injected into 0.01% AOS 1618 active surfactant concentration saturated micromodel.

smaller than those viewed in previous runs. This is significant as a similar concentration of the AOS 1618 surfactant was used, 0.01% active weight. Bubbles typically only occupied a single pore, or two to three pores after rejoining. The three fluid phases were commonly seen in contact with each other, and breaking and reforming events were viewed.

As discussed in the introduction, oil can spread as a stable layer between water and gas in the pore space. Previously trapped oil can be displaced by slow drainage through such layers. Such an event can be seen in Figure 6.1.3 from A to B. The oil apparently cannot escape from the pore and yet the air slowly displaces it. This can only happen because of drainage of an oil layer, which we cannot visualize directly. The air displaces oil in the pore over a period of one hour and forty-five minutes (6300 s). In contrast, oil re-enters the pore by direct displacement through a pore filled with oil in sequence D to E in only six seconds.

If we assume that the pressure drop driving the displacement is approximately the same in both cases, the difference must be due to the difference in conductance of a throat filled with oil and an oil layer. We may write the flow rate, q (volume per unit time), of oil into or out of the pore as:

$$q_f = \frac{\pi r^4}{8} \frac{\Delta p}{\mu L}$$

for a cylindrical throat of radius, r, filled with oil; with pressure drop Δp over a length L; and oil viscosity, μ. Imagine now that an oil layer has the following configuration in a square corner of the micromodel as depicted in Figure 6.1.4. If we assume that the oil/gas contact angle is zero, then calculations by Ransohoff and Radke (1988) give the following relation for the flow rate in a square cross-section:

$$q_L = \frac{a^4}{3.22} \frac{\Delta p}{\mu L}$$

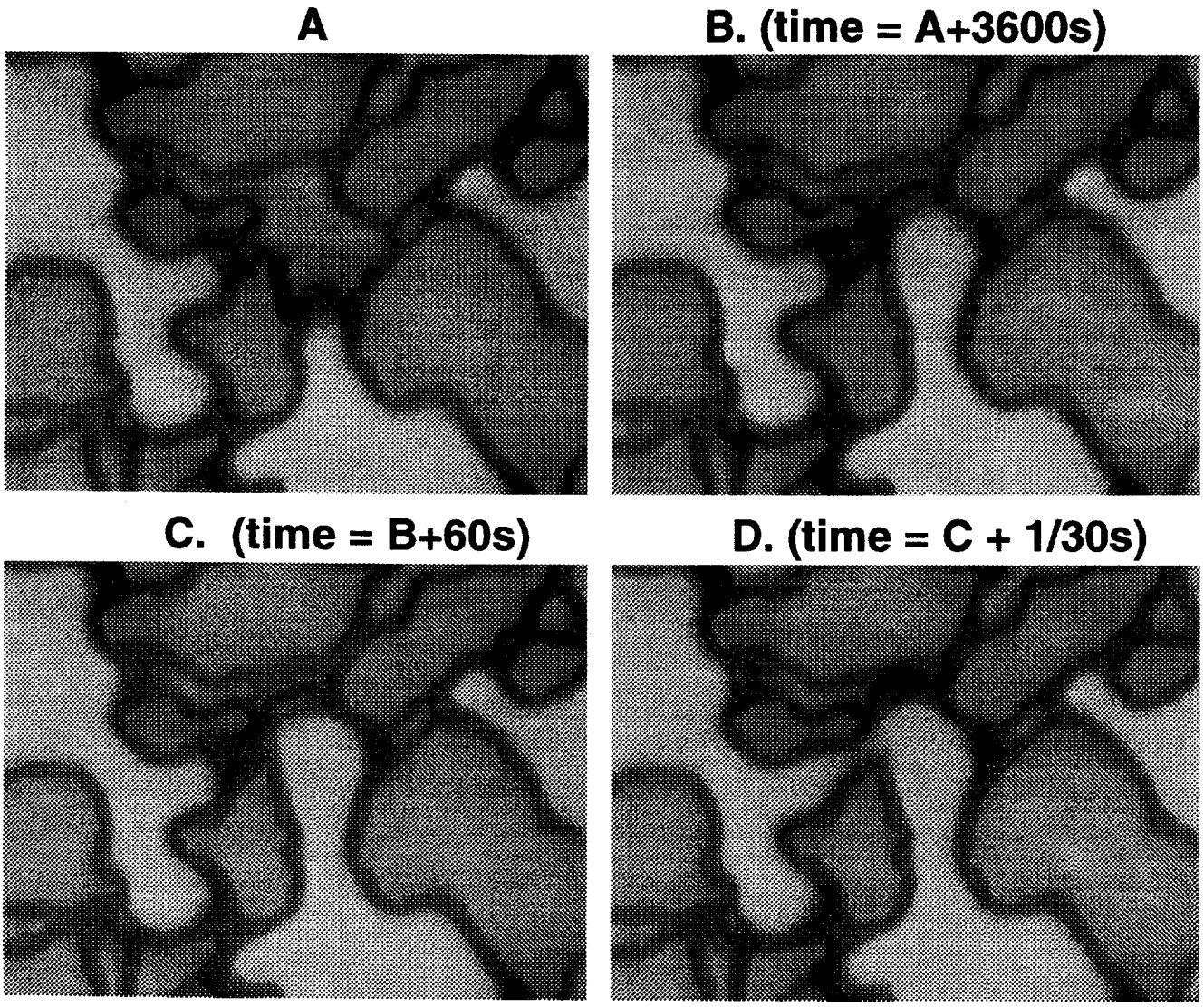

Figure 6.1.3 Air injected into decane and 0.01% AOS 1618 active surfactant concentration saturated micromodel.

where a is the thickness of the oil layer (ignoring the thickness of the water layer in the corner of the pore). The ratio of flow rates is the same as the ratio of drainage times:

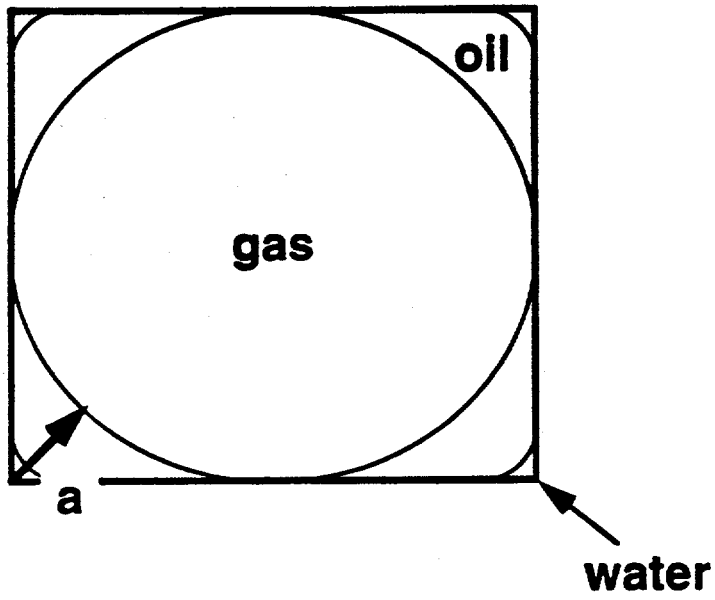

Figure 6.1.4. Schematic three phase configuration of a square corner of the silicon micromodel.

$$\frac{q_f}{q_L} = 1.26 \left(\frac{r}{a}\right)^4 = \frac{6300\ s}{0.5\ s}$$

thus,

$$\frac{r}{a} \approx 10$$

For a throat of radius approximately 7 or 8 μm, this represents a thin oil layer less than a micron across, which is very hard to visualize directly. The surfactant modifies the interfacial tensions. Without surfactant decane does not spread, but with surfactant our results imply that the spreading coefficient is positive.

Areas containing air and aqueous surfactant demonstrated an increased frequency

in foam breaking and reforming mechanisms. These events presumably occurred after the production of any residual oil contained within, although this cannot be verified. The lamellae were less stable in the presence of oil.

Pressure drop reached a maximum of 20 psig before the termination of the experiment, and exhibited less dramatic pressure fluctuations than those seen in the two phase higher air/surfactant run before. With the presence of decane maximum pressure was reduced by 23 psi. The addition of air into the system did result in further production of oil beyond the waterflood residual.

Section 6.1.4

Air/Decane/B1333

As with the AOS 1618 surfactant, residual oil saturation with the more spreading inhibitive surfactant B1333 was about 35%. The active surfactant concentration was also 0.01%. Although static three phase interactions are verified, no active interactions are seen. Instead, only oil/water and air/water interactions are seen. Increased foam generation mechanisms seemingly occur more frequently in this flouroalkyl sulfobetaine than those which happened with the alpha-olefin surfactant. This frequency of foam generation is demonstrated by the increased maximum pressure drop of 26 psig over AOS 1618. Since no Air/B1333 experiments were run, no verification of decrease in maximum pressure with residual oil can be made.

The oil phase does not interact with the foam. Although some oil was produced, we did not observe oil film drainage as in Figure 6.1.3. This implies that the oil was non-spreading in this system.

Section 6.2

Discussion

In this section, the mechanisms of propagation will be discussed. The discussion

will be divided into two subsections - one concerning two phase results, and the other three phase results.

Section 6.2.1

Two Phase Results

As seen in Figure 6.1.1, air is observed traveling in directions different from the overall direction of pressure drop - indicative of local dominance of capillary forces above viscous forces. Following the air from inlet to outlet one begins to anticipate the next pathway taken. This likely reflects air's inclination to take paths of least resistance, which is through the largest pores. More controversy exists with surfactant introduction.

Radke and Ransohoff (1986) state foam generation and propagation is accomplished primarily by the three mechanisms of snap-off, leave-behind and division. It is suggested that these mechanisms are present, under appropriate circumstances, in every medium and provide the means for air movement across the model. We did not observe snap-off in this study. Air movement was due primarily to bubble train flow. Gas moved when lamellae jumped from pore to pore. The lamellae resided in the narrowest throats and were extremely stable.

In their work on flow mechanisms, Manlowe and Radke (1990) discussed the concept of germination sites where certain pore designs made for excellent foam creating locations. Certain sites were discovered in this project where lamellae breaking and reforming occurred frequently. Figure 6.1.2 is one such site. However, no generation site lasted for long. From observations, these sites generated foam for a few minutes on average, and repeated such activity only once or twice during a typical five hour run. The bulk of the time, this sites remained dormant with partial, if not complete, liquid saturation.

Section 6.2.2

Three Phase Results

Figure 6.1.3 serves the purpose of describing two distinct processes in three phase interactions. First of all, the apparent disappearance of oil in the invaded pore suggests oil spreading as presented by Lau and O'Brien (1988). The lack of movement of the adjacent air and surfactant phases, as well as the lengthy time required to invade the body can lead one to infer oil drainage through a thin layer.

The second feature of Figure 6.1.3 is that the water/gas interfaces (or lamellae) are stable - notice the water lens between two gas filled pores in the lower left of the figure which remains stable throughout the sequence. However, we see the breakage of pseudo-emulsion films, shown from slide B to D. Once the gas has invaded the pore (with oil escaping by film drainage), there is left a water film between the oil and gas, sandwiched between two gas filled pores. It would appear that the remaining oil destabilizes the water film, allowing the gas to become connected. This appears to be consistent with the concept of pseudo-emulsion film breakage proposed by Manlowe and Radke (1990). However, the pseudo-emulsion film is stable for almost two hours between A and B and so does not collapse immediately.

Also of significance, the foam texture observed is coarser in the presence of oil. This supports the observation that oil allows the collapse of some water films.

Section 7
Conclusions

The silicon micromodels used in this project were constructed to observe, both directly and indirectly, pore level interactions of oil, air, and water. Fluid flow within the model represents two dimensional flow through a slice of Berea Sandstone. The various phase interactions were recorded visually on videotape, and are at the Stanford University Petroleum Research Institute, Stanford, California. With the termination of experiments and analysis of results, several conclusions can be drawn.

We find that the water resides in narrow regions of the pore space. The gas moves by jumping rapidly from one wide pore to another. We don't really observe lamellae as such - that is thin unstable films between gas bubbles. Because of the high water saturation, instead we observe stable water lenses. We did not see snap-off in our experiments. The 'lamellae' were stable and we saw a few breaking and reforming events, but the reforming was by liquid drainage and corner flow, rather than the classic snap-off process described by Roof (1973).

With oil, the foam was less stable, as inferred from lower pressure drops and a coarser texture. We saw events consistent with the drainage of thin spreading oil layers, we saw stable water lenses between gas and we observed the collapse of a water film between oil and gas. Further study is required to understand the full range of interactions.

References

1. Bernard, G.G., Holm, L.W., and Jacobs, W.I.:Effect of Foam on Trapped Gas Saturation and on Permeability of Porous Media to Water," SPEJ (Dec. 1965) 295-300; *Trans.* AIME, 234.

2. Bond, D.C. and Holbrook, O.C.: "Gas Drive Oil Recovery Process," US Patent No. 2,866.507 (1958).

3. Brigham, W.E.: "Injectivity Calculations for Various Flooding Patterns," P.E. 222 class notes, Stanford University, Stanford, California (1990).

4. Brigham, W.E.: "Doublets and Other Allied Well Patterns," P.E. 222 class notes, Stanford University, Stanford, California (1990).

5. Castanier, L.M. and Brigham, W.E.: "Selecting Foaming Agents for Steam Injection Improvement", *Chemical Engineering Progress* 81, No. 6 (June 1985).

6. Castanier, L.M. and Hanssen, J.E.: "Foam Mechanisms Studies", unpublished, 1995.

7. Chambers, K.T., and Radke, C.J.: "Capillary Phenomena in Foam Flow Through Porous Media," Interfacial Phenomena in Petroleum Recovery, Morrow, N.R. Es., Marcel Dekker Inc., New York (1991) Ch. 6 191-255.

8. Chen, Hsiu-Kuo and Brigham, W.E.: "Pressure Buildup for a Well with Storage and Skin in a Closed Square, *JPT* 265, (January 1978), 141-145.

9. David, A. and Marsden, S.S: "The Rheology of Foam," SPE 2544, paper presented at the SPE/AIME 44th Annual Fall Meeting, Denver (October 1969).

10. Earlougher, Robert C., Jr.: Advances in Well Test Analysis," Monograph Volume 5, Henry L. Doherty Series, Society of Petroleum Engineers of AIME, New York (1977), p. 220.

11. Fried, A.N.: "The Foam Drive Process for Increasing the Recovery of Oil," RI 5866, USBM, Washington, DC (1961).

12. Hanssen, T.M., and Jakobsen, K.R.: "Interaction of Gas-Blocking Foam with Oil in Model Porous Media," *Progress in Colloid and Polymer Science 81* (1990).

13. Harasaki, G.T. and Lawson, J.B.: "Mechanism of Foam Flow in Porous Media - Apparent Viscosity in Smooth Capillaries," SPE 12129, paper presented at the 57th Annual Technical Conference and Exhibition, San Francisco (1983),

14. Holm, L.W.: "The Mechanism of Gas and Liquid Flow Through Porous Media in the Presence of Foam," SPEJ (Dec. 1968) 359-69; *Trans.* AIME 243.

15. Hornbrook, J.W., Castanier, L.M. and Pettit, P.A.: "Observation of Foam/Oil Interactions in a New High Resolution Micromodel," SPE 22631, Paper presented at the 66th Annual Technical Conference and Exhibition, Dallas (Oct. 6-9. 1991).

16. Hornbrook, J.W., Castanier, L.M., and Pettit, P.A.: "Visualization of Foam/Oil in a New, High Resolution, Sandstone Replica Micromodel", *SUPRI TR 86*, Stanford University, August 1992.

17. Huh, D.G., Cochrane, T.S. and Kovarik, F.S.: "THe Effect of Microscopic Heterogeneity on CO2/Foam Mobility: Part 1-A Mechanistic Study,SPE 17359. paper presented at the SPE/DOE EOR Symposium, Tulsa (April 1988).

18. Jimenez, A.I. and Radke, C.J.: "Dynamic Stability of Foam Lamellae Flowing Through a Periodically Constricted Pore, " Oilfield Chemistry, Enhanced Recovery and Production Stimulation, 195th Amer. Chem. Soc. Nat. Mtg. Symp., Toronto (1989).

19. Khatib, Z.I., Hirasaki, G.J. and Falls, A.H.: "Effects of Capillary Pressure on Coalescence and Phase Mobilities in Foams Flowing Tgrough Porous Media," SPE 15442, paper presented at the 61st Annual Technical Conference and Exhibition, New Orleans (1986).

20. Kolb, G.E.: :Several Factors Affectin the Foam-Drive Process for the Removal of Water from Consolidated Porous Media," MS thesis, Penn. State U. (1964).

21. Kovscek, A.R., Patzek, T.W., and Radke, C.J.: "Mechanistic Prediction of Foam Displacement in Multidimensions: A Population Balance Approach" SPE/DOE 27789, presented at the 9th Symp. on Improved Oil Recovery, Tulsa (Apr 1994).

22. Kuhlman, M.I.: "Visualizing the Effect of Light Oil on CO2 Foams," *JPT* (July 1990) 902-908.

23. Lake, L.W.: Enhanced Oil Recovery, Prentice-Hall, Englewood Cliffs (1989).

24. Lau, H.C. and O'Brien, S.M.: "Effects of Spreaking and Nonspreading Oils on Foam Propagation Through Porous Media," *SPE Res. Eng.* (August 1988).

25. Mahmood, S.M. and Brigham, W.E.: "Two Dimensional Displacement of Oil by Gas and Surfactant Solution under Foaming Conditions," *SUPRI TR-58*, Stanford U. (July 1987).

26. Manlowe, J.D., and Radke, C.J.: "A Pore-Level Investigation of Foam/Oil Interactions in Porous Media, " *SPE Res. Eng.* (Nov. 1990).

27. Marsden, S.S.: "Foams in Porous Media", *SUPRI TR-37*, Stanford U. (1986).

28. Marsden, S.S. and Khan, S.A.: "The Flow of Foam through Short Porous Media and Apparent Viscosity Measurements (1966).

29. Mast, R.F.: "Microscopic Behavior of Foam in Porous Media", SPE 3997, paper presented at SPE Annual Fall Meeting, San Antonio (Oct. 8-11, 1972).

30. Nahid, B.H.: "Non-Darcy Flow of Gas through Porous Media in the presence of Surface Active Agents," PhD dissertation, U. of Southern California (1971).

31. Nikolov, A.D., Wasan, D.T., Huang, D.W., and Edwards, D.A.: "The Effect of Oil on Foam Stability, Mechanisms and Implications for Oil Displacement by Foam in Porous Media," SPE paper 15443 presented at the 61st Annual Technical Conference and Exhibition, New Orleans (1986).

32. Owete, O.S. and Brigham, W.E.: "Flow of Foam through Porous Media," *SUPRI TR-37*, Stanford U. (July 1984).

33. Persoff, P., Radke, C.J., Pruess, K., Bension, S.M., and Witherspoon, P.A.: "A Laboratory Investigation of Foam Flow in Sandstone at Elevated Pressure," *SPE Res. Eng.* (Aug. 1991).

34. Radke, C.J. and Ransohoff, T.C.: "Mechanisms of Foam Generation in Glass Bead Packs," SPE 15441, paper presented at the 61st Annual Technical Conference and Exhibition, New Orleans (1986).

35. Ramey, H.J., Jr., Kumar, Anil, and Gulati, Mohinder S.: "Gas Well Test Analysis Under Water-Drive Conditions," AGA, Arlington, VA (1973), pp. 312.

36. Raza, S.H. and Marsden, S.S.: "The Streaming Potential and Rheology of Foam," SPEJ (Dec. 1967) 359-68; *Trans.* AIME 240.

37. Roof, J.G.: "Snap-Off of Oil Droplets in Water-Wet Pores," *Soc. Pet. Eng. J.* (Mar. 1970). 85-90.

38. Ross, S.: "Inhibition of Foaming. II" *J. Physical & Colloid Chem.* (1950) **54**, No.3, 429.

39. Rossen, W.R.: "Chapter 12: Foams in Enhanced Oil Recovery", draft chapter in Foams: Theory, Measurements and Applications, R.K. Prud'homme and S. Khan, ed., Marcel Dekker, Inc., unpublished.

40. Sanchez, J.M. and Hazlett, R.D.: "Foam Flow through and Oil-Wet Porous Medium: A Laboratory Study", SPE 19687, paper presented at the SPE Annual Technical Conference and Exhibition, San Antonio (Oct. 8-11, 1989).

41. Sanchez, J.M. and Schechter, R.S.: "The Effect of Trace Quantities of Surfactant on Nitrogen/Water Relative Permeabilities," SPE 15446, paper presented at the 61st Annual Technical Conference and Exhibition, New Orleans (1986).

42. Sarathi, P.: "Using Micromodels to Study Steam Displacement Processes in Porous Media," NIPER-180 (1986).

43. Schramm, L.L. and Novosad, J.J.: "Microvisualization of Foam Interactions with a Crude Oil," Proc. SPE/DOE 7th Symp. on EOR, Tulsa (1990).

44. Schramm, L.L., Turta, A.T., and Novosad, J.J.: "Microvisual and Coreflood Studies of Foam Interactions with a Light Crude Oil," *SPE Res. Eng.* (Aug. 1993) 201-206.

45. Treinen, R.J., Brigham, W.E., and Castanier, L.M.: "Apparent Viscosity Measurements of Surfactant Foam in Porous Media", *SUPRI TR-48*, Report DOE/SF/11564-13, Contract No. DE86000260, U.S. DOE (Dec. 1985).

☆U.S. GOVERNMENT PRINTING OFFICE: 1996 - 760-032/20069